UDC 544.65

DOI: 10.15372/CSD2024606

EDN: HUYNEO

Layered Electrodes for Energy-Efficient Flow Vanadium Batteries

A. N. VOROPAY[1,2], E. O. DERYABINA[1], V. V. ZUEVA[1], E. D. VLADIMIR[1], E. S. OSETROV[2]

[1]*Dubna State University, Dubna, Russia*

[2]*Technocomplekt LLC, Dubna, Russia*

E-mail: voropay@uni-dubna.ru

(Received 20.01.2024; revised 26.02.2024; accepted 25.03.2024)

Abstract

Vanadium flow batteries (VFB) are becoming widespread as cheap and reliable electric storage cells. In their operating principle, VFB are very similar to fuel cells: they contain a liquid energy carrier (a rechargeable electrolyte) and a stack (a fuel cell in which an electrochemical reaction occurs). For the further development of these systems within the framework of the energy efficiency strategy, it is necessary to increase their efficiency factor, because currently it is only 60–65 %. In the present work, new electrode materials are developed and studied: combined electrodes, allowing a decrease in the internal resistance of the cell (a single element of stack design). To achieve this result, it is proposed to reduce the resistance associated with charge transfer to the electrode surface by creating an active layer with high surface area on the surface of the electrode (felt). The active layer was electrically conductive carbon black CH210, which was pre-functionalized to increase its hydrophilicity (the surface was oxidised in concentrated hydrogen peroxide at elevated pressure and temperature). Electrochemical measurements have shown that the deposition of an active layer increases the cell efficiency factor by 8.6 % at a current density of 50 mA/cm^2, which confirms the viability of this approach.

Keywords: porous electrodes, vanadium flow batteries, composites

INTRODUCTION

Vanadium flow batteries (VFB) are widely used nowadays as cheap and reliable storage cells for alternative energy sources [1] and the systems of uninterrupted power supply [2, 3]. In the operating principle, VFB are very similar to fuel cells: they contain a liquid energy carrier (a rechargeable electrolyte) and a stack (a fuel cell in which the electrochemical reaction proceeds). Up to date, VFB are the most widespread among all kinds of flow batteries, other kinds to be mentioned being the zinc-bromine batteries and organic flow batteries, currently gaining active development [4]. However, VFB attract most attention because of their distinct advantage: vanadium is an energy carrier in both the anode and cathode circuits. The reactions proceeding at the electrodes are [5]:

$$VO^{2+} + H_2O \rightleftarrows VO_2^+ + 2H^+ + e^-$$

$$V^{3+} + e^- \rightleftarrows V^{2+}$$

So, if the electrolyte crossover (transfer) from one circuit to the other occurs, vanadium ions are simply recharged according to the circuit properties. This excludes electrolyte poisoning in one circuit by the electrolyte from another one. So, if the system gets out of balance because of electro-

lyte concentrating mainly in one circuit, it may be brought back to the initial state simply by mixing the electrolyte.

The vanadium flow batteries have also other essential advantages. In particular, as they do not undergo degradation in the case of unstable charge capacity, their operation lifetime is long, and they are much more readily utilisable because of the specific features of their design. In addition, for the development of systems with maintenance time more than 4 h, VFB become economically reasonable in comparison with lithium ion batteries. However, the efficiency of VFB is 60–65 % at present, and attempts aimed at enhancement of their energy efficiency are necessary for the further development of these systems. For instance, the studies are carried out focusing on the development of new electrode materials, including carbon nanostructures, nanotubes, grapheme, ultrafine carbon [6] or with the deposition of catalytic metal oxide particles: manganese [7], nickel [8], bismuth [9]. Other approaches are based on the enhancement of battery management efficiency. Unlike for the development of new materials, when the improvement of battery parameters is a passive approach, adjustment methods form an active tool to increase the efficiency.

A flow battery consists of several main elements: a flow cell (stack), pots with the electrolyte, and pumping equipment [10]. The VFB system can also include auxiliary elements: the battery charge control system, the stack balancing system, and the voltage conversion system. For instance, the authors of [11] used the algorithm of pump productivity governing to increase the efficiency of battery performance. With this new approach, the efficiency of the system and the Coulomb efficiency increased by 3.34 and 3.84 %, respectively, in comparison with the constant flow rate. This approach is interesting because it allows solving one of the great problems, namely untimely battery disconnection, when the charge level becomes low [12], which results in the incomplete utilisation of electrolyte energy. The approach of so-called pulsed flow was used previously [13], with the pumps operating in the intermittent mode, which allowed the reduction of load on pumps by almost 50 % with a small decrease in the discharge capacity. The total efficiency of the system thus increased to more than 80 %. However, unfortunately, this approach can be destructive for the pumps because of pulsed load, which may cause the destruction of insulating material of the stator in pump motor. Expenses for pump maintenance can reach 14 % of the expenses for the maintenance of the whole system [14], and the percentage only increases within this approach. This shows that the problem of energy efficiency enhancement is still highly relevant.

In the present work, to increase the efficiency of the vanadium flow battery, the approach based on a decrease in the resistance due to the formation of an active layer with high specific surface area on the electrode surface is proposed. Unlike for the approach described in [15], the active layer is deposited not onto the whole electrode surface but only on the region near the proton-conducting membrane, to decrease the path for hydrogen ions. In this case, thus arranged active layer promotes a substantial decrease in the losses and leads to the enhancement of the energy efficiency of the system.

EXPERIMENTAL

Sample preparation

The initial electrode materials were carbon felt GFD 4.6 (SGL Carbon, Germany) and electrically conductive carbon black CH210 (Omsk Carbon Group, Russia).

The conductive carbon black CH210 was functionalised before depositing on carbon felt. At first, carbon black was placed in a muffle furnace in the air for 6 h at a temperature of 400 °C, then a 1 g portion of carbon black was put in a teflon autoclave 200 mL in volume, along with 20 mL of concentrated (25 %) hydrogen peroxide (H_2O_2, specially pure grade), and kept there at 60 °C for 48 h. Thus processed carbon black becomes hydrophilic (Fig. 1, *a*). One can see that the processed carbon black gets wet and sinks immediately, while the initial carbon black sinks only partially, while its major portion remains on the water surface and does not get wet.

After functionalisation, black carbon was mixed with the binder solution and deposited on the carbon felt. The binder solution was prepared in a vessel with a backflow condenser containing 10 mL of acetone (specially pure grade) and 0.354 g of polyvinylidene fluoride (PVDF, Gelon Lib Co., China). The mixture was stirred for 30 min at the acetone boiling point using a magnetic mixer until the complete dissolution of PVDF.

The weighted portions of 0.36 g were taken from the obtained samples of functionalised car-

bon black CH210, these portions were put in a vessel containing 20 mL of acetone, 2.25 mL of the PVDF binder, and 0.04 g of electrically conductive carbon black C45 (Gelon Lib Co., China), and mixing with an overhead stirrer was carried out for 15 min. Then the suspension was loaded into a pneumatic paint-spraying gun, and three layers were deposited onto the surface of the carbon felt electrode GFD 4.6 (see Fig. 1, *b*). The electrode temperature was maintained at 130 °C. Thus, the electrode sample FBE-4/160 was prepared (flow battery electrode (FBE) is an electrode with carbon black treated with hydrogen peroxide in the autoclave for 4 h at 160 °C).

For comparison, FBE-0 (initial felt without deposition) was used.

Electrochemical tests

Electrochemical tests were carried out in a two-electrode cell (the general view of the assembled cell is presented in Fig. 1, *c*, and the model of a cell with spaced elements is shown in Fig. 1, *d*) in the galvanostatic mode using an Elins P20X8 potentiostat (Elins, Russia) at the current of 156, 313, 469 and 625 mA, which corresponds to the current density of 25, 50, 75 and 100 mA/cm^2. The electrodes were mounted so that the active layer was directed at the proton-conducting membrane. The voltage ranged from 0.9 to 1.6 V. The electrode thickness was 4 mm.

The solution containing a mixture of vanadium ions and sulphuric acid was used as the electrolyte. According to the results reported in [16], the optimal composition of the electrolyte was: 0.8 mol/L VO^{2+}, 0.8 mol/L V^{3+} and 3 mol/L SO_4^{2-}. The composition was confirmed over the intensities of the corresponding absorption bands of vanadium ions in the optical density spectra (Fig. 2), as described in [17]. For VO^{2+} ions, the characteristic absorption band is observed at 760 nm, while for V^{3+} ions at 400 nm. The optical density was measured using an SF-2000 spectrophotometer (OKB SPEKTR, Russia). Then the two-electrode cells were filled with the electrolyte, sealed (to

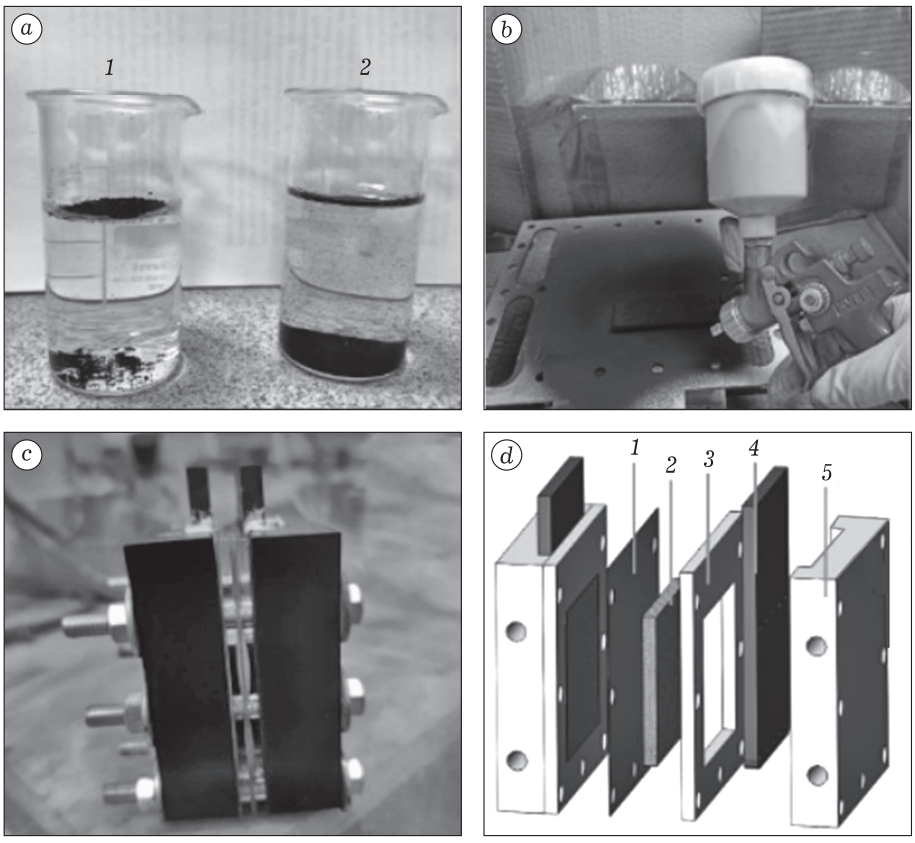

Fig. 1. Photographs of: *a* – carbon black CH210 before (*1*) and after (*2*) functionalisation; *b* – deposition of the active layer on the surface of carbon felt; *c* – the general view of the assembled measurement cell; *d* – 3D-models of measurement cell (*1* – proton-conducting membrane Nafion 117; *2* – porous electrode; *3* – housing plate; *4* – graphite electrode; *5* – external housing of the cell).

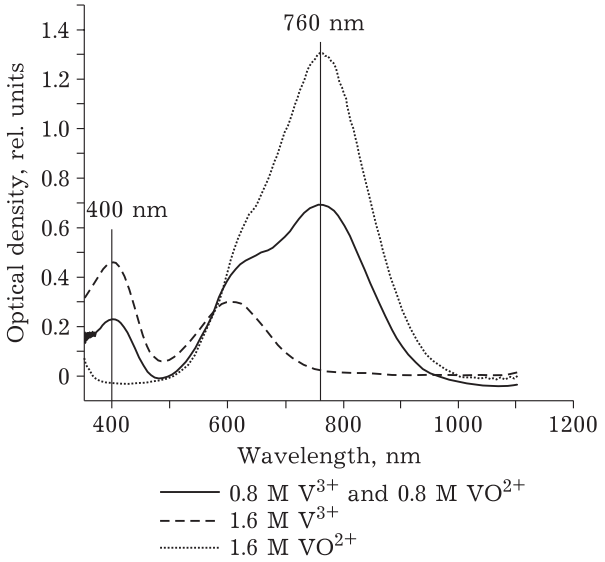

Fig. 2. The optical density spectra of initial vanadium electrolyte and reference solutions of vanadium (1.6 M VO^{2+} and 1.6 M V^{3+}).

exclude oxygen access), and measurements were carried out without electrolyte pumping.

The charge and discharge capacity was determined from the curves obtained in the galvanostatic mode using the equation

$$E = \int_0^t U(t)I(t)\mathrm{d}t \quad (1)$$

The energy efficiency was calculated using the equation

$$\eta(E) = \frac{E_{\text{disch}}}{E_{\text{ch}}} \quad (2)$$

while the Coulomb efficiency and voltage efficiency were calculated using the equations

$$\eta(Q) = \frac{Q_{\text{disch}}}{Q_{\text{ch}}} \quad (3)$$

$$\eta(U) = \frac{\eta(E)}{\eta(Q)} \quad (4)$$

The area specific resistance of the cell (assembled as electrode/Nafion 117/electrode) was determined similarly to [5], from the total energy losses according to the equation

$$\text{ASR} = \frac{(E_{\text{ch}} - E_{\text{disch}})}{I^2(t_{\text{ch}} + t_{\text{disch}})} S \quad (5)$$

where E_{disch} and E_{ch} are discharge and charge energy, respectively, J; t_{disch} and t_{ch} are discharge and charge times, respectively, s; I is current at which the measurement is made, A; Q_{disch} and Q_{ch} are the electric charges of discharge and charge, respectively, C; ASR is the area specific resistance, Ohm · cm^2; S is the electrode surface area, m^2; U_{disch} is the starting discharge voltage, V.

Impedance spectra were recorded at the frequency within the range from 1 MHz to 1 mHz with the voltage amplitude of 20 mV using a Bio-Logic SP-200 potentiostat (France) at the electrode voltage of 1.5 V (open-circuit voltage).

RESULTS AND DISCUSSION

The photographs of samples taken using optical microscopy are shown in Fig. 3. One can see that the active layer contains cracks (see Fig. 3, *a*) and coarse inhomogeneities, but along with that, it is rather dense. Carbon felt looks like a nonwoven highly porous material (see Fig. 3, *b*).

The charge-discharge curves for samples FBE-0 and FBE-4/160 are shown in Fig. 4. The plots are normalised for the charging time (t_{ch}) of each sample. This procedure is necessary for the obvious comparison of samples excluding the effect of electrolyte volume because the amount of

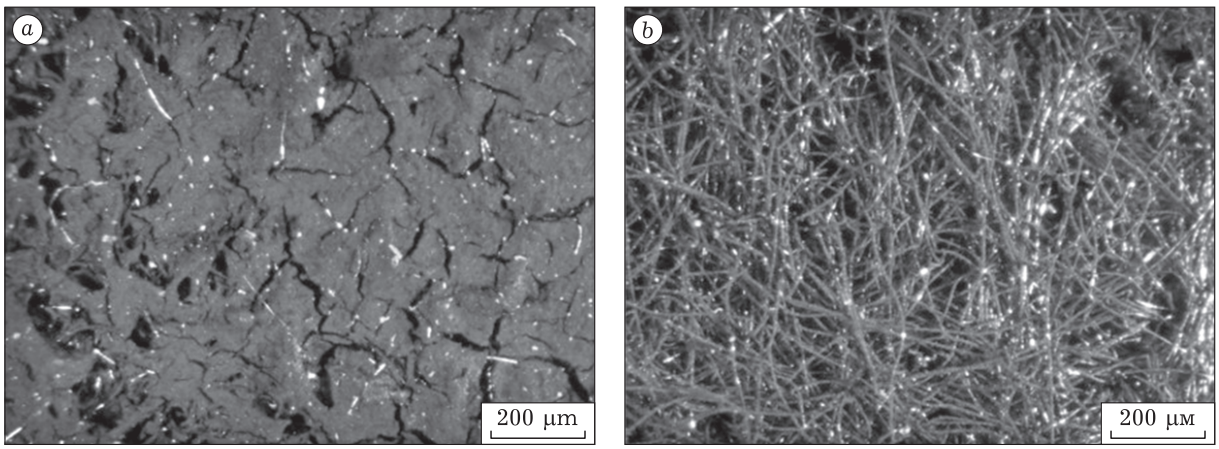

Fig. 3. Photographs of the surface of samples FBE-4/160 (*a*) and FBE-0 (*b*).

electrolyte in each cell may slightly differ. This is because the electrolyte is not only in the electrode volume but also in the input channels of the cell, while a definite portion of the electrolyte can be removed from the channels during preservation.

One can see in Fig. 4 that the curve of charging voltage for the FBE-0 sample goes above that for FBE-4/160, suggesting a higher internal resistance of the FBE-0 sample. Estimating from the charge-to-discharge switching voltage drop, we obtain that the internal resistance of FBE-0 is almost twice as high as that of FBE-4/160.

The results of efficiency calculation for the samples under study are presented in Fig. 5. Thus, the charge efficiency (see Fig. 5, *a*) for the samples is below 100 %, which is due to the self-discharge of cells, caused by vanadium ion diffusion through the proton-conducting membrane [18, 19] depending on discharge time. Capacity losses can also be due to overvoltage in the cell because of the non-uniform potential on the electrode surface [20]. Membrane size is the same in all samples, so larger energy losses in the FBE-0 sample may be related exactly with the non-uniform distribution of the potential over electrode surface, which is expressed as a decrease in the voltage efficiency for the sample without an active layer (see Fig. 5, *b*). The result is a higher energy efficiency for FBE-4/160 sample (see Fig. 5, *c*), and an increase in the efficiency is non-uniform: it reaches the maximal value at the current density of 50 mA/cm^2.

The area specific resistance (ASR) and the depth of discharge (w), that is, the capacity factor (the ratio of discharge capacity to the total discharge capacity) depending on the working current are presented in Table 1. The total discharge capacity was accepted to be the discharge value at the current 156 mA for this sample. One can see that the capacity factor w increases for the

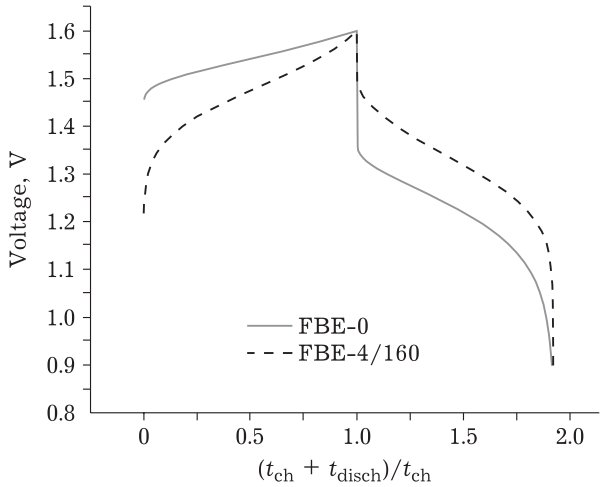

Fig. 4. Charge-discharge curves normalised for charging time at the current density of 50 mA/cm^2.

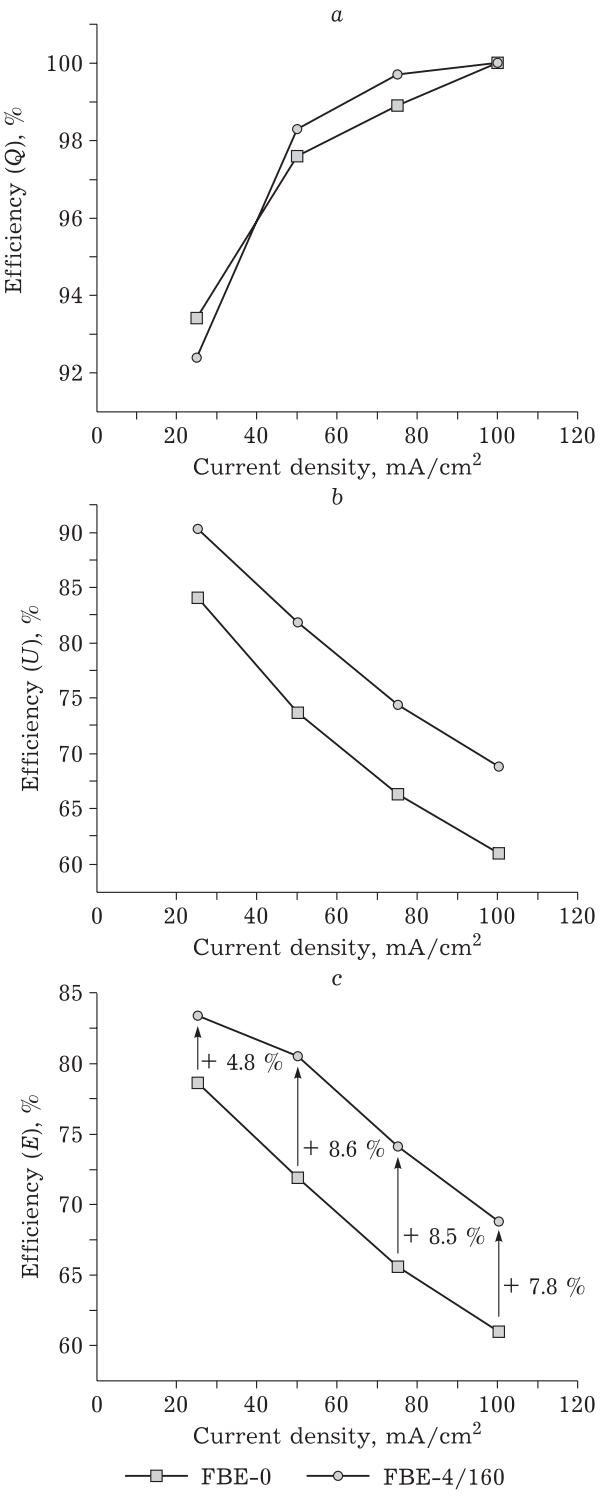

Fig. 5. Dependences of the output efficiency of samples under investigation on the current density: *a* – charge efficiency (Q); *b* – voltage efficiency (U); *c* – energy efficiency (E).

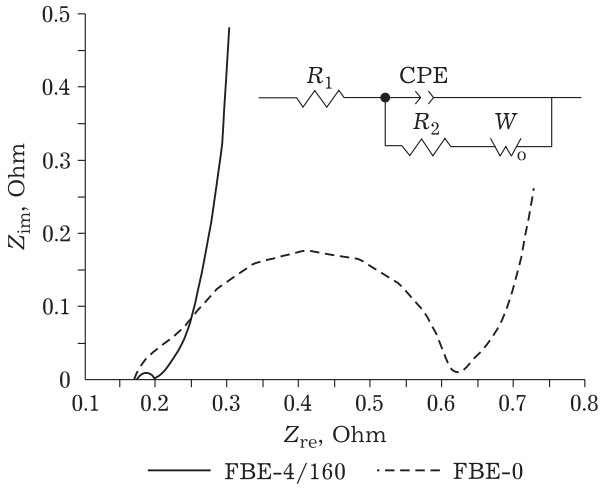

Fig. 6. Nyquist diagrams of the samples FBE-4/160 and FBE-0. The equivalent circuit to calculate the impedance (*Z*) is shown in the insert.

electrodes with the active layer, which is extremely important for flow batteries, as this parameter determines the energy output ratio of the electrolyte in the resulting system [21, 22].

The area surface resistance decreases for the cell with the deposited active layer, which is finally the reason of a substantial increase in the energy efficiency of the cell in comparison with initial carbon felt.

The Nyquist diagrams fort he studied samples are shown in Fig. 6. The impedance (*Z*) was calculated according to the equivalent circuit (see Fig. 6, insert). The circuit was chosen similarly to [23–25].

One can see that the FBE-4/160 sample possesses lower resistance, which has also been indirectly confirmed by the above-mentioned ASR data (see Table 1). However, analysis of impedance spectra (calculation parameters are presented in Table 2) shows that resistance R_2 and the W-T parameter (the ratio of squared diffusion layer thickness to the diffusion coefficient) decrease, while CPE-P parameter slightly increases.

An increase in the CPE-P parameter can be explained by a sharp increase in the surface area of the electrode, which causes the imbalance of electrode properties towards the capacitor. More interesting parameters are R2 and W-T. Most probably, a decrease in W-T is associated with the counterwork of two factors: a decrease in the diffusion coefficient due to a decrease in pore size in the active layer, a decrease in the diffusion path length due to higher developed surface and a smaller pore size in the active layer. However, the factor related to a decrease in the thickness of the diffusion layer is more distinctly pronounced, which leads to a decrease in W-T parameter for FBE-4/160 sample. A similar effect was observed in [26–28], but the ions of the electrolyte penetrated the pores inside the fibres in those works. The effect of the active layer is also pronounced as a decrease in R2. Most probably, this decrease in explained by an increase in the specific surface area of the electrode, which causes a decrease in the charge transfer resistance on the electrodes.

CONCLUSION

Thus, we have demonstrated the operability of the concept of combined electrodes for vanadium flow batteries, leading to a substantial increase in the cell efficiency (from 60.8 to 80.5 %) and the capacity factor (from 4.7 to 20.2 %). Most likely, the reason is a decrease in the losses related to a decrease in the charge transfer resistance on the electrode surface due to an increase

TABLE 1

Dependence of discharge depth (*w*) and area surface resistance (ASR) of the samples on the working current

Current, mA	FBE-0		FBE-4/160	
	w, %	ASR, Ohm · cm^2	*w*, %	ASR, Ohm · cm^2
156	100	6.63	100	5.05
313	55.8	4.43	75.1	2.95
469	21.0	3.61	43.9	2.64
625	4.7	3.06	20.2	2.41

TABLE 2

Parameters for the calculation of impedance of the samples

Parameter	FBE-0	FBE-4/160
R_1	0.186	0.175
CPE-P	0.85	0.98
R_2	0.427	0.018
W-R	0.26	0.25
W-T	166	80

Note. R_1 and R_2 are resistance values at different regions of the circuit (see Fig. 6, insert); CPE-P – the index of power in the CPE element (for CPE-P = 1, the element is a capacitor); W-R – the frequency-independent part of Warburg impedance; W-T – the ratio of the squared thickness of diffusion layer to the diffusion coefficient.

in the surface area of the active layer. This assumption is confirmed by the results of impedance spectroscopy exhibiting a decrease in the value of R_2 parameter from 0.427 to 0.018 Ohm.

REFERENCES

1 Alotto P., Guarnieri M., Moro F., Redox flow batteries for the storage of renewable energy: a review, *Renewable Sustainable Energy Rev.*, 2014, Vol. 29, P. 325–335.

2 Voropay A. N., Kuz'min I. N., Loskutov A. B., Osetrov E. S., A flow battery based source for autonomous power supply systems, *Elektrichestvo*, 2022, No. 9, P. 45–52. (In Russ.).

3 Belov D. V., Voropay A. N., Kuz'min I. N., Loskutov A. B., Studying the effect the characteristics and design of electric energy storage devices have on the operation of uninterruptible power supply systems, *Elektrichestvo*, 2020, No. 10, P. 4–11. (In Russ.).

4 Ramar A., Wang F.-M., Foeng R., Hsing R., Organic redox flow battery: are organic redox materials suited to aqueous solvents or organic solvents?, *J. Power Sources*, 2023, Vol. 558, Art. 232611.

5 Komarov V. A., Voropay A. N., Il'ina M. N., Goryacheva T. V., Research of nanostructured carbon felt materials as electrodes of vanadium flow batteries, *Rus. J. Electrochem.*, 2021, Vol. 57, No. 8, P. 892–897.

6 Nair U. R., Costa-Castelló R., A model predictive control-based energy management scheme for hybrid storage system in islanded microgrids, *IEEE Access*, 2020, Vol. 8, P. 97809–97822.

7 Zhang Z., Xi J., Zhou H., Qiu X., KOH etched graphite felt with improved wettability and activity for vanadium flow batteries, *Electrochim. Acta*, 2016, Vol. 218, P. 15–23.

8 Kim K. J., Park M.-S., Kim J. H., Hwang U., Lee N. J., Jeong G., Kim Y. J., Novel catalytic effects of Mn_3O_4 for all vanadium redox flow batteries, *Chem. Commun.*, 2012, Vol. 48, No. 44, P. 5455–5457.

9 Park J. J., Park J. H., Park O. O., Yang J. H., Highly porous graphenated graphite felt electrodes with catalytic defects for high-performance vanadium redox flow batteries produced via NiO/Ni redox reactions, *Carbon*, 2016, Vol. 110, P. 17–26.

10 González Z., Sánchez A., Blanco C., Granda M., Menéndez R., Santamaría R., Enhanced performance of a Bi-modified graphite felt as the positive electrode of a vanadium redox flow battery, *Electrochem. Commun.*, 2011, Vol. 13, P. 1379–1382.

11 Encyclopedia of Energy Storage, L. F. Cabeza (Ed.), Vol. 2, Electrochemical Storage, Elsevier, Amsterdam, 2022, P. 407–422

12 Xiao W., Tan L., Control strategy optimization of electrolyte flow rate for all vanadium redox flow battery with consideration of pump, *Renewable Energy*, 2019, Vol. 133, P. 1445–1454.

13 Ma X., Zhang H., Sun C., Zou Y., Zhang T., An optimal strategy of electrolyte flow rate for vanadium redox flow battery, *J. Power Sources*, 2012, Vol. 203, P. 153–158.

14 Ling C. Y., Cao H., Chng M. L., Han M., Birgersson E., Pulsating electrolyte flow in a full vanadium redox battery, *J. Power Sources*, 2015, Vol. 294, P. 305–311.

15 Wei L., Zhao T. S., Zhao G., An L., Zeng L., A high-performance carbon nanoparticle-decorated graphite felt electrode for vanadium redox flow batteries, *Appl. Energy*, 2016, Vol. 176, P. 74–79.

16 Rashitov I., Voropay A., Tsepilov G., Kuzmin I., Loskutov A., Kurkin A., Osetrov E., Lipuzhin I., Vanadium redox flow battery stack balancing to increase depth of discharge using forced flow attenuation, *Batteries*, 2023, Vol. 9, No. 9, Art. 464.

17 Loktionov P., Pichugov R., Konev D., Petrov M., Pustovalova A., Antipov A., Operando UV/Vis spectra deconvolution for comprehensive electrolytes analysis of vanadium redox flow battery, *J. Electroanal. Chem.*, 2022, Vol. 925, Art. 116912.

18 Düerkop D., Widdecke H., Schilde C., Kunz U., Schmiemann A., Polymer membranes for all-vanadium redox flow batteries: a review, *Membranes*, 2021, Vol. 11, No. 3, Art. 214.

19 Sankaralingam R. K., Seshadri S., Sunarso J., Bhatt A. I., Kapoor A., Overview of the factors affecting the performance of vanadium redox flow batteries, *J. Energy Storage*, 2021, Vol. 41, Art. 102857.

20 Zhu M., Wu Q., Chi X., Luo Y., Simulation of all-vanadium redox flow batteries based on COMSOL, in: 29th Chinese Control and Decision Conference (2017CCDC), 28–30 May 2017, Chongqing, China, IEEE Industrial Electronics, Singapore, 2017, P. 6977–6982.

21 Sun C., Vezzù K., Pagot G., Nale A., Bang Y. H., Pace G., Negro E., Gambaro C., Meda L., Zawodzinski T. A., Di Noto V., Elucidation of the interplay between vanadium species and charge-discharge processes in VRFBs by Raman spectroscopy, *Electrochim. Acta*, 2019, Vol. 318, P. 913–921.

22 Ali E., Kim J., Park H., Numerical analysis of modified channel widths of serpentine and interdigitated channels for the discharge performance of vanadium redox flow batteries, *J. Energy Storage*, 2022, Vol. 53, Art. 105099.

23 Liu T., Li X., Zhang H., Chen J., Progress on the electrode materials towards vanadium flow batteries (VFBs) with improved power density, *J. Energy Chem.*, 2018, Vol. 27, No. 5, P. 1292–1303.

24 Friedl J., Bauer C. M., Rinaldi A., Stimming U., Electron transfer kinetics of the VO^{2+}/VO_2^+-reaction on multi-walled carbon nanotubes, *Carbon*, 2013, Vol. 63, P. 228–239.

25 Li Y., Bao J., Skyllas-Kazacos M., Akter M. P., Zhang X., Fletcher J., Studies on dynamic responses and impedance of the vanadium redox flow battery, *Appl. Energy*, 2019, Vol. 237, P. 91–102.

26 Wu L., Wang J., Shen Y., Liu L., Xi J., Electrochemical evaluation methods of vanadium flow battery electrodes, *Phys. Chem. Chem. Phys.*, 2017, Vol. 19, No. 22, P. 14708–14717.

27 Wang R., Li Y., Liu H., He Y.-L., Hao M., Sandwich-like multi-scale hierarchical porous carbon with a highly hydroxylated surface for flow batteries, *J. Mater. Chem. A*, 2021, Vol. 9, No. 4, P. 2345–2356.

28 Jiang H. R., Sun J., Wei L., Wu M. C., Shyy W., Zhao T. S., A high power density and long cycle life vanadium redox flow battery, *Energy Storage Mater.*, 2020, Vol. 24, P. 529–540.